

# Quantum State Designs with Clifford Enhanced Matrix Product States

Guglielmo Lami,<sup>1</sup> Tobias Haug,<sup>2</sup> and Jacopo De Nardis<sup>1</sup>

<sup>1</sup>Laboratoire de Physique Théorique et Modélisation, CNRS UMR 8089,  
CY Cergy Paris Université, 95302 Cergy-Pontoise Cedex, France

<sup>2</sup>Quantum Research Center, Technology Innovation Institute, Abu Dhabi, UAE

Nonstabilizerness, or ‘magic’, is a critical quantum resource that, together with entanglement, characterizes the non-classical complexity of quantum states. Here, we address the problem of quantifying the average nonstabilizerness of random Matrix Product States (RMPS). RMPS represent a generalization of random product states featuring bounded entanglement that scales logarithmically with the bond dimension  $\chi$ . We demonstrate that the 2-Stabilizer Rényi Entropy converges to that of Haar random states as  $N/\chi^2$ , where  $N$  is the system size. This indicates that MPS with a modest bond dimension are as magical as generic states. Subsequently, we introduce the ensemble of Clifford enhanced Matrix Product States (CMPS), built by the action of Clifford unitaries on RMPS. Leveraging our previous result, we show that CMPS can approximate 4-spherical designs with arbitrary accuracy. Specifically, for a constant  $N$ , CMPS become close to 4-designs with a scaling as  $\chi^{-2}$ . Our findings indicate that combining Clifford unitaries with polynomially complex tensor network states can generate highly non-trivial quantum states.

*Introduction.*— Quantum states of many interacting particles (or qubits) are very complex, since they typically require exponential resources to be simulated [1–5] or learned [6]. Nevertheless, at least two broad categories of quantum states that can be simulated classically are known.

Firstly, states exhibiting limited amount of quantum correlations between their constituencies, i.e. low entanglement, can be simulated efficiently by means of Tensor Networks [7–12]. Their one-dimensional version, Matrix Product States (MPS) involves contracting  $N$  matrices of size  $\chi$ , where  $\chi$  represents the bond dimension and  $N$  the number of qubits. Entanglement scales as  $\log \chi$ , ensuring efficiency as long as entanglement remains bounded [13].

However, while entanglement is a crucial quantum resource, it is not sufficient for classical hardness. Stabilizer states, formed by the Clifford group acting on computational basis states, may exhibit high entanglement but remain simulatable and learnable with polynomial complexity [14–26]. The Clifford group entails unitary operations mapping Pauli operators into Pauli operators [14]. Generic quantum states can be formed by combining Clifford operations and non-Clifford resource states, where the latter are regarded as a key quantum resource for fault-tolerant quantum computation [14, 27]. The resource theory of nonstabilizerness (aka quantum magic) has been introduced to quantify the extent to which a state deviates from being constructed solely with Cliffords [27–30]. States with sufficiently low magic can be simulated using the tableau formalism [14–17, 31–34]. However, simulations (such as sampling in the computational basis) can become inefficient when Cliffords interact with a large number of magic resource states [32]. States obtained with random Cliffords applied to magical resource have attracted considerable interest, and average values of physical quantities such as multi-fractal flatness [35], out-of-time-order correlators [36, 37] and en-

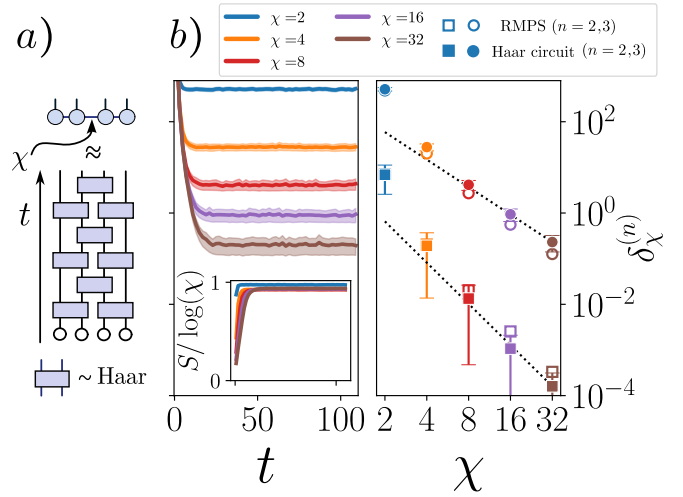


Figure 1. *a)* A random circuit comprising two local random unitary is considered. The initial state evolves as an MPS, with the bond dimension growing up to  $\chi$ . *b)* Left: convergence of the magic with the MPS bond dimension ( $N = 22$  qubits, 500 trajectories). Deviation of the  $n$ -SRE ( $n = 2$ ) from the averaged Haar value,  $\delta_\chi^{(n)}$ , is plotted over discrete circuit time  $t$ . (Inset: maximum entanglement entropy  $S$  of the evolved MPS). Right:  $\delta_\chi^{(n)}$  ( $n = 2, 3$ ) for the final state compared with exact RMPS average obtained for the same size and  $\chi$ . Black lines represents power laws  $\chi^{-2}$  and  $\chi^{-3}$ .

tanglement spectrum flatness [38] are directly linked to the nonstabilizerness of the resource state.

In this paper we focus on a broader class of magical resource states, namely Matrix Product States (MPS). Indeed, identifying effective methods to combine MPS with Clifford circuits and characterizing the resulting states presents an intriguing and largely unexplored prospect, with potential implications for classical simulation capabilities.

*Main results.*— We focus on typical states resulting from the action of a Clifford unitary on a generic MPS. To characterize such an ensemble, we employ the formalism of random Matrix Product States (RMPS) [39–44]. RMPS can be taken as generalisation of random product states with finite entanglement scaling as  $\log \chi$ , where  $\chi$  is the bond dimension. First, we show that for RMPS with open boundary conditions, the Stabiliser Rényi Entropies (SRE) [29], a widely used measure of non-stabilizerness, approach their average value for random Haar-distributed states with deviations  $\mathcal{O}(N/\chi^2)$  for Rényi index  $n = 2$ , and  $\mathcal{O}(N/\chi^3)$  for Rényi index  $n = 3$ . As illustrated in Fig. 1, this behavior can be visualized by evolving an MPS under a random Haar circuit [45] truncated to bond dimension  $\chi$ . Entanglement entropy  $S$  rapidly reaches its maximum value  $\log \chi$  (see inset). Similarly, the SRE approaches a  $\chi$ -dependent value, converging polynomially quickly to the Haar state values. We then investigate how the ensemble generated by applying random Clifford operators to RMPS (CMPS) approximates Haar states. For this purpose, we adopt the concept of  $k$ -spherical design, a property of state ensembles reproducing Haar averages up to the  $k$ -th moment. Stabilizer states form exact 3-designs [19], approximate 4-designs, and are far from 6-designs [46]. Although the deviation from 4-design decreases exponentially with the number  $N$  of qubits [46, 47], for fixed  $N$  this may not be sufficiently small in practice. Indeed, stabilizers do not reproduce important universal features of Haar states, having for instance exponentially larger purity fluctuations [36]. Here, we show that for CMPS the deviation from 4-design can be arbitrarily reduced by increasing  $\chi$ , with deviations that scale as  $N\chi^{-2}$ . Given the complexity of computing  $k$ -folded Clifford channels for  $k > 4$ , we cannot predict higher moments, yet achieving a 4-design with arbitrary accuracy is significant. Indeed, we prove that the inherent simplicity of MPS and Cliffords, when combined, can produce highly non-trivial quantum states, featuring the same entanglement, purity fluctuations, and magic as typical quantum states.

*Preliminaries.*— We consider a system consisting of  $N$  qubits. The Hilbert space, of size  $d = 2^N$ , is locally spanned by the basis states  $|s_i\rangle \in \{|0\rangle, |1\rangle\}$  ( $i = 1, 2, \dots, N$ ).  $\mathcal{U}(d)$  is the corresponding group of unitary operators. The Haar measure  $\mu_{\text{H}}$  is the unique left/right invariant measure over  $\mathcal{U}(d)$  [48]. Expectation values over Haar are denoted as  $\mathbb{E}_{\mathcal{U} \sim \mu_{\text{H}}}[\dots] \equiv \int d\mu_{\text{H}}(\dots)$ . For any ensemble of unitaries  $\mathcal{X}$ , we can define the uniform probability distribution over it  $\mu_{\mathcal{X}}$ . Expectation values can be computed as  $\mathbb{E}_{\mathcal{U} \sim \mu_{\mathcal{X}}}[\dots] \equiv 1/|\mathcal{X}| \cdot \sum_{\mathcal{U} \in \mathcal{X}}(\dots)$ . An ensemble of unitaries that satisfies

$$\mathbb{E}_{\mathcal{U} \sim \mu_{\mathcal{X}}}[(\mathcal{U}^\dagger)^{\otimes k} O(\mathcal{U})^{\otimes k}] = \mathbb{E}_{\mathcal{U} \sim \mu_{\text{H}}}[(\mathcal{U}^\dagger)^{\otimes k} O(\mathcal{U})^{\otimes k}] \quad (1)$$

for any operator  $O$  acting on  $k$  replicas of the system is called  $k$ -design. Intuitively,  $k$ -designs are distributions of

unitaries that replicate the moments of the Haar measure up to the  $k$ -th order. Similarly, if now  $\mathcal{X}$  represent a set of states  $\{|\psi\rangle\}$ , one can introduce the notion of  $k$ -spherical design. This refers to an ensemble for which

$$\mathbb{E}_{\psi \sim \mu_{\mathcal{X}}}[(|\psi\rangle\langle\psi|)^{\otimes k}] = \mathbb{E}_{\psi \sim \mu_{\text{H}}}[(|\psi\rangle\langle\psi|)^{\otimes k}]. \quad (2)$$

If  $\mathcal{X}$  is a  $k$ -unitary design then the ensemble of states  $\mathcal{X}|\mathbf{0}\rangle$ , with  $|\mathbf{0}\rangle \equiv \bigotimes_{j=1}^N |0\rangle$ , is a  $k$ -spherical design. The frame potential of  $\mathcal{X}$  is defined as [19, 48–50]

$$\begin{aligned} \mathcal{F}_{\mathcal{X}}^{(k)} &= \mathbb{E}_{\psi, \psi' \sim \mu_{\mathcal{X}}} [|\langle\psi'|\psi\rangle|^{2k}] = \\ &= \mathbb{E}_{\psi, \psi' \sim \mu_{\mathcal{X}}} [\text{Tr}[(|\psi'\rangle\langle\psi'|)^{\otimes k} (|\psi\rangle\langle\psi|)^{\otimes k}]]. \end{aligned}$$

It can be proven that  $\mathcal{F}_{\mathcal{X}}^{(k)} \geq \mathcal{F}_{\text{H}}^{(k)}$ , where  $\mathcal{F}_{\text{H}}^{(k)} = \binom{d+k-1}{k}^{-1}$  is the frame potential of the Haar distribution and the equality holds only if  $\mathcal{X}$  is a  $k$ -spherical design.

We denote the Pauli operators as  $\{\sigma^\alpha\}_{\alpha=0}^3 = \{\mathbb{1}, X, Y, Z\}$ , and with  $\sigma = \bigotimes_{j=1}^N \sigma_j$  a generic tensor product of them, i.e. a Pauli string. Pauli strings  $\tilde{\mathcal{P}}_N = \{\sigma\}_\sigma$ , with appropriate global phases constitute the Pauli group  $\mathcal{P}_N = (\pm 1, \pm i)\tilde{\mathcal{P}}_N$ . The Clifford group  $\mathcal{C}(d)$  consists of  $N$ -qubits unitaries  $\mathcal{U}_c$  preserving the Pauli group under conjugation, i.e.  $\mathcal{C}(d) = \{\mathcal{U}_c \in \mathcal{U}(d) \text{ s.t. } \mathcal{U}_c^\dagger \mathcal{P}_N \mathcal{U}_c = \mathcal{P}_N\}$ .  $\mu_{\mathcal{C}}$  represents the uniform probability distribution over the Clifford group, as defined before. Hadamard  $H$ , phase  $S$ , and CNOT gates collectively generate the complete group [14]. To approximate any  $N$ -qubit unitary and achieve universality, an additional gate such as the single-qubit  $T$  gate  $T = \text{diag}(1, e^{i\pi/4})$  is required [14]. States obtained by applying Cliffords to  $|\mathbf{0}\rangle$  are known as stabilizer states, and its set is denoted as  $\text{STAB} = \{\mathcal{U}_c|\mathbf{0}\rangle\}_{\mathcal{U}_c}$ . There exist classical efficient algorithms to simulate stabilizer states, thanks to a tableau algorithm (Gottesman-Knill theorem) [14–17].

*Clifford and Haar averages.*— The Clifford group  $\mathcal{C}(d)$  constitutes a 3-unitary design [51], and therefore  $\mathbb{E}_{\mathcal{U}_c \sim \mu_{\mathcal{C}}}[(\mathcal{U}_c^\dagger)^{\otimes k} O(\mathcal{U}_c)^{\otimes k}] = \mathbb{E}_{\mathcal{U} \sim \mu_{\text{H}}}[(\mathcal{U}^\dagger)^{\otimes k} O(\mathcal{U})^{\otimes k}]$  for  $k \leq 3$ . Consequently, the set of stabilizer states constitutes a 3-spherical design [19]. The  $k$ -fold Haar channel  $\mathbb{E}_{\mathcal{U} \sim \mu_{\text{H}}}[(\mathcal{U}^\dagger)^{\otimes k} O(\mathcal{U})^{\otimes k}]$  can be computed thanks to the Weingarten calculus [48, 52], giving

$$\mathbb{E}_{\mathcal{U} \sim \mu_{\text{H}}}[(\mathcal{U}^\dagger)^{\otimes k} O(\mathcal{U})^{\otimes k}] = \sum_{\sigma, \pi \in S_k} \text{Wg}(\sigma^{-1}\pi, d) \text{Tr}[OT_\sigma]T_\pi, \quad (3)$$

where  $T_\sigma, T_\pi$  are unitary representations of the permutations  $\sigma, \pi \in S_k$  acting on  $k$  replicas of the system, and  $\text{Wg}$  are the Weingarten functions. For any normalized state  $|\psi\rangle$  and  $O = (|\psi\rangle\langle\psi|)^{\otimes k}$ , Eq. 3 simplifies to  $\mathbb{E}_{\mathcal{U} \sim \mu_{\text{H}}}[(\mathcal{U}^\dagger|\psi\rangle\langle\psi|\mathcal{U})^{\otimes k}] = P_{\text{symm}}^{(k)}/\text{Tr}[P_{\text{symm}}^{(k)}]$ , with  $P_{\text{symm}}^{(k)} = \sum_{\pi \in S_k} T_\pi/k!$  the projector onto the symmetric subspace of the permutation group  $S_k$  and  $\text{Tr}[P_{\text{symm}}^{(k)}] = \binom{k+d-1}{k}$ . As a significant application, we mention the

calculation of the purity of a reduced density matrix  $P_A(|\psi\rangle) = \text{Tr}_A[\rho_A^2]$ ,  $\rho_A = \text{Tr}_B[\rho]$  corresponding to a generic system bipartition  $A, B$  averaged over the ensemble of pure stabilizer states  $\rho = |\psi\rangle\langle\psi|$ ,  $|\psi\rangle \in \text{STAB}$ . First, we rewrite the purity as  $P_A(|\psi\rangle) = \text{Tr}[\rho^{\otimes 2} T_{21}^{(A)}]$ , where  $T_{21}^{(A)}$  is the permutation (swap) operator exchanging replicas 1 and 2 of subsystem  $A$  (while acting as the identity on  $B$ ). Therefore

$$\mathbb{E}_{\psi \sim \text{STAB}} [P_A(|\psi\rangle)] = \text{Tr} \left[ \mathbb{E}_{\mathcal{U}_c \sim \mu_c} [(\mathcal{U}_c^\dagger |\mathbf{0}\rangle \langle \mathbf{0}| \mathcal{U}_c)^{\otimes 2}] T_{21}^{(A)} \right], \quad (4)$$

A straightforward computation therefore gives

$$\mathbb{E}_{\psi \sim \text{STAB}} [P_A(|\psi\rangle)] = \frac{d_A + d_B}{d_A d_B + 1} = \frac{2\sqrt{d}}{d+1} \sim \frac{2}{\sqrt{d}}, \quad (5)$$

where second equalities holds for  $d_A = d_B = d^{1/2}$ . Since the Rényi-2 entanglement entropy is  $S_2(\rho_A) = -\log P_A(|\psi\rangle)$ , and  $\mathbb{E}[S_2(\rho_A)] \geq -\log \mathbb{E}[P_A(|\psi\rangle)]$ , this result shows that stabilizer states have in average the same entanglement of random states, i.e. close to the maximum value (which is given by the maximally mixed state  $\rho_A = \mathbb{1}/\sqrt{d}$ ).

The 4-fold Clifford channel is also known [18]. In particular

$$\mathbb{E}_{\mathcal{U}_c \sim \mu_c} [(\mathcal{U}_c^\dagger |\psi\rangle \langle \psi| \mathcal{U}_c)^{\otimes 4}] = \alpha_\psi Q P_{\text{symm}}^{(4)} + \beta_\psi P_{\text{symm}}^{(4)} \quad (6)$$

where  $Q = d^{-2} \sum_{\sigma \in \mathcal{P}_N} \sigma^{\otimes 4}$  and the factors  $\alpha_\psi$  and  $\beta_\psi$  are

$$\alpha_\psi = \frac{6d(d+3)\|\Pi_\psi\|_2^2 - 24}{(d^2-1)(d+2)(d+4)} \quad \beta_\psi = \frac{24(1-\|\Pi_\psi\|_2^2)}{(d^2-1)(d+2)(d+4)}. \quad (7)$$

with  $\Pi_\psi(\sigma) = d^{-1} \langle \psi | \sigma | \psi \rangle^2$  being a vector of length  $d^2$ . Note that  $\Pi_\psi(\sigma)$  sums to 1, since  $d^{-1} \sum_{\sigma \in \mathcal{P}_N} \langle \psi | \sigma | \psi \rangle^2 = \text{Tr}[\rho^2] = 1$ , so  $\Pi_\psi$  is a probability distribution [29], sometimes referred to as a characteristic function [18].

Using this result, it is possible to compute the fluctuations of purity for stabilizer states [36]. These are defined as:

$$\Delta^2 P_A(|\psi\rangle) = \mathbb{E}[P_A(|\psi\rangle)^2] - \mathbb{E}[P_A(|\psi\rangle)]^2, \quad (8)$$

where the second term, as shown before, is the same for Clifford and Haar random states, while the first term can be computed via Eq.6 (see Suppl.Mat. for details). One gets (with  $d_A = d_B = d^{1/2}$ ) [36]

$$\Delta^2 P_A(|\psi\rangle)|_{\text{STAB}} = \frac{(d-1)^2}{(d+1)^2(d+2)} \sim \mathcal{O}(d^{-1}), \quad (9)$$

whereas the result for Haar states is

$$\Delta^2 P_A(|\psi\rangle)|_{\text{H}} = \frac{2(d-1)^2}{(d+1)^2(d+2)(d+3)} \sim \mathcal{O}(d^{-2}) \quad (10)$$

Therefore, stabilizer states have exponentially larger purity fluctuations compared to Haar states [36].

*Nonstabilizerness.*— Nonstabilizerness (magic) is regarded as a veritable resource for quantum systems and computation, both theoretically and practically [14–17, 27, 31–34]. In a nutshell, nonstabilizerness is the resource required for quantum states to be unattainable through Clifford circuits (plus Pauli measurements). The latter are regarded as easy to implement free operations, while non-Clifford gates are resources. Several measures of nonstabilizerness have been proposed [30, 53, 54].

Here, we utilize the Stabilizer Rényi Entropies (SRE), originally introduced in Ref. [29], which have gained significant attention for their potential in analytical [55, 56] and numerical [57–61] evaluation, as well as their applicability to experimental measurements [26, 37], and their relevance to many-body quantum systems [33, 57, 58, 62–65]. SRE, indexed by a  $n$ -Rényi index, are the entropies of the characteristic probability distribution  $\Pi_\psi(\sigma)$  (excluding an additive constant). If we introduce the  $(n-1)$ -moment of  $\Pi_\psi$  ( $n > 1$ ) as

$$m_n(|\psi\rangle) = \|\Pi_\psi\|_n^n = d^{-n} \sum_{\sigma} \langle \psi | \sigma | \psi \rangle^{2n}, \quad (11)$$

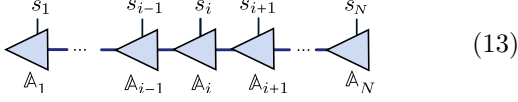
the  $n$ -SRE is given by  $\mathcal{M}_n(|\psi\rangle) = (1-n)^{-1} \log m_n(|\psi\rangle) - \log d$ , while its linearized version  $\mathcal{M}_n^{\text{lin}}(|\psi\rangle) = 1 - d^{n-1} m_n$  is essentially  $m_n$ , apart from irrelevant constants. SREs exhibit the following properties [29, 66], accordingly being a good measure of nonstabilizerness: i)  $\mathcal{M}_n \geq 0$  ( $m_n \leq d^{1-n}$ ), with equality holding iff  $|\psi\rangle \in \text{STAB}$ ; ii) SREs are invariant under Clifford unitaries; iii) they are additive. Recently, for pure states the monotonicity of SRE for  $n \geq 2$  has been rigorously established [66], and it has been shown that  $\mathcal{M}_n^{\text{lin}}$  serves as a strong monotone for the same range of  $n$ . On the other hand, a violation of monotonicity for  $0 \leq n < 2$  has been reported in systems undergoing measurements in the computational basis [60]. Finally, SREs provide useful bounds for other measures of magic [66]. The evaluation of SREs for MPS has been explored both through a replica approach [59–61] and through efficient estimation obtained with a sampling in the Pauli basis [57, 58]. However, the question of how SREs converge with respect to the bond dimension  $\chi$  has not been addressed until now. Here, we offer a solution leveraging the RMPS framework.

*Random Matrix Product States (RMPS).*— MPS [8–10] are a class of quantum many-body states characterized by bounded entanglement entropy. MPS are defined as

$$|\phi\rangle = \sum_{s_1, s_2, \dots, s_N} \mathbb{A}_1^{s_1} \mathbb{A}_2^{s_2} \dots \mathbb{A}_N^{s_N} |s_1, s_2, \dots, s_N\rangle, \quad (12)$$

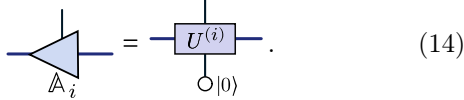
with  $\mathbb{A}_j^{s_j}$  being  $\chi_{j-1} \times \chi_j$  matrices, except at the left (right) boundary where  $\mathbb{A}_1^{s_1}$  ( $\mathbb{A}_N^{s_N}$ ) is a  $1 \times \chi_1$  ( $\chi_{N-1} \times 1$ ) row

(column) vector. MPS can be graphically represented as [8–10]



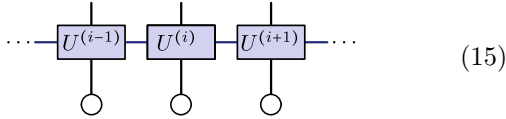
$$\begin{array}{c} s_1 \quad s_{i-1} \quad s_i \quad s_{i+1} \quad s_N \\ \triangleleft \quad \triangleleft \quad \triangleleft \quad \triangleleft \quad \triangleleft \\ \mathbb{A}_1 \quad \mathbb{A}_{i-1} \quad \mathbb{A}_i \quad \mathbb{A}_{i+1} \quad \mathbb{A}_N \end{array} \quad (13)$$

Without loss of generality, the tensors  $\mathbb{A}$  can be assumed to be isometries, satisfying the right-normalization condition  $(\mathbb{A}_i^{s_i})_{\alpha\beta}(\mathbb{A}_i^{s_i,*})_{\alpha'\beta} = \delta_{\alpha\alpha'}$ , where indices  $\alpha, \alpha', \beta$  run in the auxiliary space, which has dimension  $\chi$  (bond dimension) [8]. Isometries  $\mathbb{A}_i$  can be embedded into larger unitary matrices  $U^{(i)}$  of size  $q = 2\chi$ . The embedding is such that  $(\mathbb{A}_i^{s_i})_{\alpha\beta} = \langle 0\alpha|U^{(i)}|s_i\beta\rangle$ , i.e.



$$\begin{array}{c} \triangleleft \\ \mathbb{A}_i \end{array} = \begin{array}{c} \square \\ U^{(i)} \\ \circ |0\rangle \end{array} \quad (14)$$

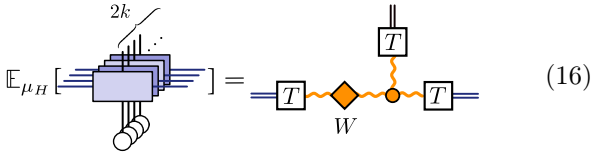
As a result, an MPS with maximum bond dimension  $\chi$  (assuming  $\chi$  is a power of 2) is equivalent to a quantum circuit comprising sequential unitaries  $U^{(i)}$  acting on, at most,  $\log_2 \chi + 1$  qubits initialized to  $|0\rangle$  [67–70], i.e.



$$\dots \begin{array}{c} \square \\ U^{(i-1)} \\ \circ \end{array} \begin{array}{c} \square \\ U^{(i)} \\ \circ \end{array} \begin{array}{c} \square \\ U^{(i+1)} \\ \circ \end{array} \dots \quad (15)$$

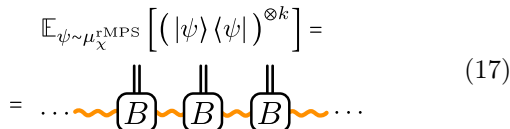
At this point, one can introduce a probability measure  $\mu_\chi$  for RMPS by requiring the generating unitaries to be Haar random, i.e.  $U^{(i)} \sim \mu_H$  [39–42]. It should be noted, however, that using  $N$  unitaries of the same dimension as in the bulk typically yields unnormalized states, with normalization only restored for large  $N$  [42]. When handling finite  $N$ , implementing suitable boundary conditions, with smaller sizes for unitaries at the edges, might be beneficial (details in Suppl.Mat.).

The  $k$ -fold RMPS channel  $\mathbb{E}_{\psi \sim \mu_\chi}[(|\psi\rangle\langle\psi|)^{\otimes k}]$  can be constructed by tensorizing  $k$  replicas of the Haar matrices  $U, U^*$  (the latter indicated by darker shapes in the following pictures) and applying Eq. 3. The result is [41]



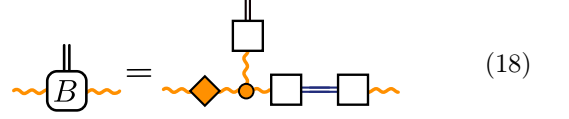
$$\mathbb{E}_{\mu_H}[\dots] = \begin{array}{c} \square \\ T \\ \square \\ W \end{array} \quad (16)$$

Here, we used double lines to represent physical or auxiliary indices tensorized over the replicas, and wavy orange lines to represent permutation indices  $\pi \in S_k$ . The tensor  $T$  contains all permutation operators  $T_\pi$ , folded as vectors [41].  $W$  is the Weingarten matrix  $W_{\sigma\pi} = \text{Wg}(\sigma^{-1}\pi, q)$  [52]. We obtain therefore



$$\begin{aligned} \mathbb{E}_{\psi \sim \mu_\chi^{\text{rMPS}}}[(|\psi\rangle\langle\psi|)^{\otimes k}] &= \\ &= \dots \begin{array}{c} \square \\ B \end{array} \begin{array}{c} \square \\ B \end{array} \begin{array}{c} \square \\ B \end{array} \dots \end{aligned} \quad (17)$$

where the MPS replicated blocks are defined as [41]



$$\begin{array}{c} \square \\ B \end{array} = \begin{array}{c} \square \\ \diamond \\ \circ \\ \square \end{array} \quad (18)$$

Note that auxiliary indices are contracted within the matrices  $B$ , which have size  $k!$ , independently of  $\chi$  [41]. Therefore one can easily access the large  $\chi$  limit.

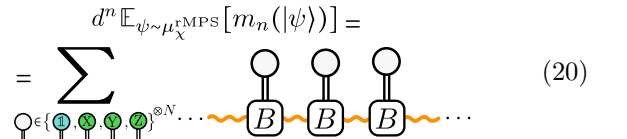
By examining explicitly the block Eq. 18 for  $k = 1$ , one can easily show that RMPS are 1-spherical design [40] for any  $\chi \geq 1$ . However, RMPS fail to be spherical 2-designs [42], since they have inherently low-entanglement,  $\mathbb{E}_{\psi \sim \mu_\chi}[\text{P}_A(|\psi\rangle)] \geq \chi^{-1}$ , while for Haar states the average purity is exponentially small (Eq. 5).

Finally we mention that RMPS can be prepared with precision  $\epsilon$  using circuits of depth  $\mathcal{O}(\log(N/\epsilon))$  [71]. For translationally invariant MPS, the preparation can be improved using adaptive circuits that achieve a constant depth, independent of  $N$  [72].

*Magic of RMPS*— We can now compute the average value of the linearized  $n$ -SRE over the ensemble of RMPS (a similar computations has been performed in Ref. [41, 44]). The case  $\chi = 1$ , i.e. random product states, is particularly simple (see Suppl.Mat.) and gives:  $d^2 \mathbb{E}_{\psi \sim \mu_{\chi=1}}[m_2(|\psi\rangle)] = d^{\log_2(8/5)}$ . The general case needs to be treated with the Weingarten formalism introduced above. We have

$$d^n \mathbb{E}_{\psi \sim \mu_\chi}[m_n(|\psi\rangle)] = \sum_{\sigma} \text{Tr}[\sigma^{\otimes k} \mathbb{E}_{\psi \sim \mu_\chi}[(|\psi\rangle\langle\psi|)^{\otimes k}]], \quad (19)$$

where  $k = 2n$ . Local Pauli operators  $\sigma_i^{\otimes k}$  can be folded as vectors and contracted with physical indices of the block  $B$  in Eq. 17. We thus obtain



$$\begin{aligned} d^n \mathbb{E}_{\psi \sim \mu_\chi^{\text{rMPS}}}[m_n(|\psi\rangle)] &= \\ &= \sum_{\sigma \in \{\text{Pauli}\}^{\otimes N}} \dots \begin{array}{c} \square \\ B \end{array} \begin{array}{c} \square \\ B \end{array} \begin{array}{c} \square \\ B \end{array} \dots \end{aligned} \quad (20)$$

After factorizing the Pauli sum, one can introduce the following transfer matrix  $\mathcal{T}$



$$\begin{array}{c} \square \\ \mathcal{T} \end{array} = \sum_{\sigma \in \{\text{Pauli}\}} \begin{array}{c} \square \\ \sigma \end{array} \quad (21)$$

so that Eq.20 becomes



$$d^n \mathbb{E}_{\psi \sim \mu_\chi^{\text{rMPS}}}[m_n(|\psi\rangle)] = \dots \begin{array}{c} \square \\ \mathcal{T} \end{array} \begin{array}{c} \square \\ \mathcal{T} \end{array} \begin{array}{c} \square \\ \mathcal{T} \end{array} \dots \quad (22)$$

Matrix elements of  $\mathcal{T}$  can be determined through symbolic computation, and consist of rational functions of  $\chi$ .

Boundary conditions can be implemented in two distinct ways:

$$\begin{array}{l} a) \\ b) \end{array} \quad \left( \begin{array}{c} \text{---} \text{---} \text{---} \text{---} \text{---} \\ \text{---} \text{---} \text{---} \text{---} \text{---} \end{array} \right), \quad (23)$$

namely open boundary conditions, *a*), or open boundary conditions, *b*). The first approach leads to  $d^n \mathbb{E}_{\phi \sim \mu_\chi} [m_n(|\phi\rangle)] = \text{Tr}[\mathcal{T}^N]$ , which is easy to handle, since the calculation boils down to finding the eigenvalues of  $\mathcal{T}$  in the bulk. We determine them through a semi-analytical calculation for large  $\chi$ : for  $n = 2$  the four leading eigenvalues converge to 1 as  $N/\chi^2$ , while for  $n = 3$  the only leading eigenvalue converges to 1 as  $N/\chi^6$ . In both cases, all the other eigenvalues converge to lower values in  $[0, 1)$ , being irrelevant for  $N \gg 1$ . Consequently, for  $n = 2$  we have  $\text{Tr}[\mathcal{T}^N] \simeq (1 + a\chi^{-2})^N + 3(1 - b\chi^{-2})^N$ , with  $a = 9/4$ ,  $b = 3/4$ . An expansion for large  $\chi$  results into

$$\text{Tr}[\mathcal{T}^N] \simeq 4 + \frac{27}{8} \left( \frac{N}{\chi^2} \right)^2. \quad (24)$$

It is useful to define

$$\delta_\chi^{(n)} = d^n \left( \mathbb{E}_{\phi \sim \mu_\chi} [m_n(|\phi\rangle)] - \mathbb{E}_{\phi \sim \mu_H} [m_n(|\phi\rangle)] \right), \quad (25)$$

which measures the average deviation of the  $n$ -linearized magic from that of Haar states. The factor  $d^n$  in Eq. 25 is included to ensure that the Haar average is of  $\mathcal{O}(1)$ . Indeed for  $n = 2, 3$  and large  $d$  one has  $d^2 \mathbb{E}_{\phi \sim \mu_H} [\|\Pi_\phi\|_2^2] \simeq 4$  and  $d^3 \mathbb{E}_{\phi \sim \mu_H} [\|\Pi_\phi\|_3^3] \simeq 1$  (see Suppl.Mat.). By replacing  $d^n \mathbb{E}_{\phi \sim \mu_\chi} [m_n(|\phi\rangle)]$  with Eq. 24 and subtracting the Haar value, we obtain  $\delta_\chi^{(2)} \sim \mathcal{O}\left(\frac{N}{\chi^2}\right)$ . This implies that when  $\chi \gg N^{1/2}$ , the 2-linearized magic of the RMPS converges to that of Haar, i.e.  $\delta_\chi^{(2)}$  approaches 0. With similar arguments, we show that  $\delta_\chi^{(3)} \sim \mathcal{O}\left(\frac{N}{\chi^6}\right)$ , i.e. the 3-linearized magic converges for  $\chi \gg N^{1/6}$ .

However, it should be noted that evaluating the average SRE as in Eq. 23a) is not exact, as for finite  $N$ , RMPS obtained with periodic boundary conditions are not properly normalized [42]. Hence, we improved the calculation by considering open boundary condition to enforce state normalization (see Suppl.Mat. for details). In this scenario,  $\mathcal{T}$  varies across sites, and the SRE is obtained by multiplying the matrices as in Eq. 23 b). A numerical evaluation for  $\chi \in [2, 16384]$ ,  $N \in [4, 2048]$  shows that in this case the scaling is  $\delta_\chi^{(2)} \sim \mathcal{O}\left(\frac{N}{\chi^2}\right)$  and  $\delta_\chi^{(3)} \sim \mathcal{O}\left(\frac{N}{\chi^3}\right)$  (see Suppl.Mat.).

To alternatively confirm this scenario, we simulated the evolution of a circuit with 2-qubit Haar random unitaries, allowing the MPS bond dimension to grow up

to  $\chi$  (see Fig. 1 a). We measure  $\delta_\chi^{(n)}$  for  $n = 2, 3$  and observe power law decays of  $\chi^{-2}$  and  $\chi^{-3}$ , consistent with predictions from finite-size RMPS calculation (see Fig. 1 b).

*Clifford enhanced RMPS*– We are now in position to introduce a novel ensemble of quantum states, dubbed CMPS. These are defined as

$$\text{CMPS} = \{|\psi\rangle = \mathcal{U}_c |\phi\rangle_\chi, \mathcal{U}_c \in \mathcal{C}(d) \text{ and } |\phi\rangle_\chi \in \text{MPS}\},$$

i.e. by applying a Clifford circuit to an MPS with maximum bond dimension  $\chi$ . Note that arbitrary CMPS can be prepared using circuits of depth  $\mathcal{O}(N)$ , as this is the depth required by generic Clifford unitaries [73]. The depth of CMPS can be reduced to  $\mathcal{O}(\log(n))$  by restricting to Clifford constructions that form 2-designs [74] and normal MPS [71, 72].

Hereafter, we use  $\mathbb{E}[\dots]$  to denote average over CMPS, i.e. over both Clifford  $\mathcal{U}_c$  and MPS  $|\phi\rangle_\chi$ , the latter equipped with the measure  $\mu_\chi$ .

First, it is trivial to show that CMPS inherit from  $\mathcal{C}(d)$  the property of being (spherical) 3-design. Indeed, for any  $k \leq 3$ , we have

$$\begin{aligned} \mathbb{E}[(|\psi\rangle\langle\psi|)^{\otimes k}] &= \mathbb{E}_{\phi \sim \mu_\chi} [\mathbb{E}_{\mathcal{U} \sim \mu_C} [(\mathcal{U}^\dagger |\phi\rangle\langle\phi| \mathcal{U})^{\otimes k}]] = \\ &= \mathbb{E}_{\phi \sim \mu_\chi} [\mathbb{E}_{\mathcal{U} \sim \mu_H} [(\mathcal{U}^\dagger |\phi\rangle\langle\phi| \mathcal{U})^{\otimes k}]] = \mathbb{E}_{\psi \sim \mu_H} [(|\psi\rangle\langle\psi|)^{\otimes k}]. \end{aligned} \quad (26)$$

Thus, to detect deviations of the CMPS ensemble from Haar, we must study fourth moments. In order to quantify these deviations, we evaluate the CMPS 4-frame potential

$$\mathcal{F}_{\text{CMPS}}^{(4)} = \mathbb{E} \left[ \text{Tr} [(\mathcal{U}_c^\dagger |\phi\rangle\langle\phi| \mathcal{U}_c)^{\otimes 4} (\mathcal{V}_c^\dagger |\varphi\rangle\langle\varphi| \mathcal{V}_c)^{\otimes 4}] \right], \quad (27)$$

where we average over Clifford  $\mathcal{U}_c, \mathcal{V}_c$  and RMPS  $|\phi\rangle, |\varphi\rangle$ . By using the normalized Schatten-2 distance from Haar [50, 75]  $\Delta^{(k)} = (\mathcal{F}^{(k)} / \mathcal{F}_H^{(k)} - 1)^{1/2}$  (which is an upper bound to the trace-distance deviation), and using Eq. 6, we get

$$\Delta^{(4)} = \frac{d+3}{d} \frac{1}{(4(d-1)(4+d))^{1/2}} \delta_\chi^{(2)} \sim \frac{1}{2d} \delta_\chi^{(2)}. \quad (28)$$

Another way to quantify the closeness of CMPS to Haar is calculating the fluctuations of purity (Eq. 8) and verifying how these interpolate between the Clifford regime  $\Delta^2 \text{P}_A|_{\text{STAB}} \sim \mathcal{O}(d^{-1})$  and the Haar regime  $\Delta^2 \text{P}_A|_H \sim \mathcal{O}(d^{-2})$  (Eqs. 9, 10). By exploiting again Eq. 6, one gets (see Suppl.Mat. for details)

$$\Delta^2 \text{P}_A(|\psi\rangle) = \Delta^2 \text{P}_A(|\psi\rangle)|_H + \frac{(d-1)}{d(d+1)(d+2)} \delta_\chi^{(2)}. \quad (29)$$

In summary, both the computation of the 4-frame potential and the analysis of purity fluctuations boil

down to evaluating  $\delta_\chi^{(2)}$ . Consequently, the way the ensemble  $\mathcal{U}_c|\phi\rangle$  becomes close to Haar random states depends on the magic of the states  $|\phi\rangle$  (in our case RMPS). For  $\chi = 1$ , one finds  $\delta_\chi^{(2)} \sim \mathcal{O}(d^{\log_2(8/5)})$  and therefore,  $\Delta^2 P_A(|\psi\rangle) \sim \mathcal{O}(d^{1-\log_2 5})$ . This indicates that random product states enhanced by Clifford circuits still exhibit exponentially larger purity fluctuations compared to those of Haar random states. However, as shown in previous section, for any fixed  $N$ ,  $\delta_\chi^{(2)}$  can be made arbitrarily small by increasing  $\chi$ . The closeness to a 4-design  $\Delta^{(4)}$  can be reduced in the same way. More specifically, for a given  $N$  and any  $\epsilon > 0$ , achieving  $\Delta^{(4)} < \epsilon$  requires that  $\chi > \frac{1}{\sqrt{2\epsilon}} \sqrt{\frac{N}{d}}$ .

*Conclusions and Outlook*— We have given new insights into the relationship between two fundamental quantum resources: entanglement and magic. Specifically, we demonstrated that MPS, which inherently possess bounded entanglement, when enhanced by the application of Clifford (magic-free) unitaries, can yield highly non-trivial quantum states that exhibit characteristics akin to those of generic Haar states. We denoted CMPS the ensemble of states  $|\psi\rangle = \mathcal{U}_c|\phi\rangle_\chi$ , where  $|\phi\rangle_\chi$  is an MPS and  $\mathcal{U}_c$  a Clifford. By appropriately adjusting the MPS bond dimension  $\chi$ , one can achieve an approximate 4-design with arbitrary precision, which scales as  $\chi^{-2}$ .

The question of whether CMPS representation could enhance classical simulations of many-body quantum systems or quantum circuits by effectively combining the MPS and Clifford (tableau) formalism remains open [76]. While sampling CMPS in the computational basis is likely challenging [32], one can efficiently compute the expectation value of any Pauli string  $\sigma$ . This efficiency arises as  $\langle\psi|\sigma|\psi\rangle = \langle\phi|\sigma'|\phi\rangle$ , where  $\sigma' = \mathcal{U}_c^\dagger \sigma \mathcal{U}_c$ . We can efficiently compute  $\langle\psi|\sigma|\psi\rangle$  by using the Clifford tableau formalism to transform  $\sigma$  into  $\sigma'$ . This is followed by contracting the MPS to evaluate  $\langle\phi|\sigma'|\phi\rangle$ , which can be done in  $\mathcal{O}(N\chi^3)$  time. In Suppl.Mat. we show how a circuit of two-qubit Clifford unitaries can be used to largely decrease the entanglement of a highly entangled state. The latter is obtained by evolving an initial product state with a random  $T$ -doped Clifford circuit. This fact, known as entanglement cooling, was already pointed out in [77] and it shows how elements in the ensemble  $\mathcal{U}_c|\psi\rangle$  can be successfully used to reproduce a complex states  $|\psi\rangle$ . Extending the entanglement cooling to target MPS with bond dimension  $\chi$  polynomial in  $N$ , as well as developing analogous MPS-Clifford techniques, represents a formidable challenge for future research. Such approaches, if realized, could prove particularly effective for tasks that require only the computation of Pauli expectation values, such as determining ground states or simulating the time evolution of Hamiltonians [3, 78, 79]. Finally, it would be interesting to understand whether the CMPS representation of a given

state  $|\psi\rangle$  can be efficiently learned [80].

*Acknowledgments.* – We are particularly grateful to L. Piroli for useful advices on RMPS calculations. We also want to thank A. Paviglianiti, M. Collura, A. Hamma, L. Tagliacozzo and A. De Luca for inspiring discussions and for collaborations on topics connected with this work. This work was supported by ANR-22-CPJ1-0021-01 and ERC Starting Grant 101042293 (HEPIQ).

*Note added*— While finalizing this work, we became aware of a related study on the convergence of magic with bond dimension in MPS representing ground states. The paper, authored by M.Frau, P.S.Tarabunga, M.Collura, M.Dalmonte, E.Tirrito, will appear on the same arxiv posting.

- 
- [1] R. P. Feynman, Simulating physics with computers, *International Journal of Theoretical Physics* **21**, 467 (1982).
  - [2] W. Kohn, Nobel Lecture: Electronic structure of matter—wave functions and density functionals, *Rev. Mod. Phys.* **71**, 1253 (1999).
  - [3] A. J. Daley, I. Bloch, C. Kokail, S. Flannigan, N. Pearson, M. Troyer, and P. Zoller, Practical quantum advantage in quantum simulation, *Nature* **607**, 667 (2022).
  - [4] X. Xu, S. Benjamin, J. Sun, X. Yuan, and P. Zhang, A Herculean task: Classical simulation of quantum computers (2023), [arXiv:2302.08880 \[quant-ph\]](https://arxiv.org/abs/2302.08880).
  - [5] H. Pashayan, S. D. Bartlett, and D. Gross, From estimation of quantum probabilities to simulation of quantum circuits, *Quantum* **4**, 223 (2020).
  - [6] A. Anshu and S. Arunachalam, A survey on the complexity of learning quantum states (2023), [arXiv:2305.20069 \[quant-ph\]](https://arxiv.org/abs/2305.20069).
  - [7] G. Vidal, Efficient Simulation of One-Dimensional Quantum Many-Body Systems, *Phys. Rev. Lett.* **93**, 040502 (2004).
  - [8] U. Schollwöck, The density-matrix renormalization group in the age of matrix product states, *Annals of Physics* **326**, 96 (2011), january 2011 Special Issue.
  - [9] P. Silvi, F. Tschirsich, M. Gerster, J. Jünemann, D. Jaschke, M. Rizzi, and S. Montangero, The Tensor Networks Anthology: Simulation techniques for many-body quantum lattice systems, *SciPost Physics Lecture Notes* [10.21468/scipostphyslectnotes.8](https://arxiv.org/abs/10.21468/scipostphyslectnotes.8) (2019).
  - [10] J. Biamonte, Lectures on Quantum Tensor Networks (2020), [arXiv:1912.10049 \[quant-ph\]](https://arxiv.org/abs/1912.10049).
  - [11] J. I. Cirac, D. Pérez-García, N. Schuch, and F. Verstraete, Matrix product states and projected entangled pair states: Concepts, symmetries, theorems, *Reviews of Modern Physics* **93**, [10.1103/revmodphys.93.045003](https://arxiv.org/abs/10.1103/revmodphys.93.045003) (2021).
  - [12] J. Tindall, M. Fishman, E. M. Stoudenmire, and D. Sels, Efficient Tensor Network Simulation of IBM’s Eagle Kicked Ising Experiment, *PRX Quantum* **5**, 010308

- (2024).
- [13] M. B. Hastings, An area law for one-dimensional quantum systems, *Journal of Statistical Mechanics: Theory and Experiment* **2007**, P08024–P08024 (2007).
- [14] M. A. Nielsen and I. L. Chuang, *Quantum Computation and Quantum Information: 10th Anniversary Edition* (Cambridge University Press, 2010).
- [15] D. Gottesman, *Stabilizer Codes and Quantum Error Correction* (1997).
- [16] D. Gottesman, Theory of fault-tolerant quantum computation, *Phys. Rev. A* **57**, 127 (1998).
- [17] D. Gottesman, The Heisenberg Representation of Quantum Computers, arXiv preprint arXiv:9807006 [10.48550/ARXIV.QUANT-PH/9807006](https://arxiv.org/abs/10.48550/ARXIV.QUANT-PH/9807006) (1998).
- [18] H. Zhu, R. Kueng, M. Grassl, and D. Gross, The Clifford group fails gracefully to be a unitary 4-design (2016), [arXiv:1609.08172](https://arxiv.org/abs/1609.08172) [quant-ph].
- [19] R. Kueng and D. Gross, Qubit stabilizer states are complex projective 3-designs (2015), [arXiv:1510.02767](https://arxiv.org/abs/1510.02767) [quant-ph].
- [20] S. Grewal, V. Iyer, W. Kretschmer, and D. Liang, Efficient Learning of Quantum States Prepared With Few Non-Clifford Gates (2023), [arXiv:2305.13409](https://arxiv.org/abs/2305.13409) [quant-ph].
- [21] M. Beverland, E. Campbell, M. Howard, and V. Kliuchnikov, Lower bounds on the non-Clifford resources for quantum computations, *Quantum Science and Technology* **5**, 035009 (2020).
- [22] J. Jiang and X. Wang, Lower Bound for the T Count Via Unitary Stabilizer Nullity, *Physical Review Applied* **19**, [10.1103/physrevapplied.19.034052](https://doi.org/10.1103/physrevapplied.19.034052) (2023).
- [23] A. Montanaro, Learning stabilizer states by Bell sampling (2017), [arXiv:1707.04012](https://arxiv.org/abs/1707.04012) [quant-ph].
- [24] J. Iaconis, Quantum state complexity in computationally tractable quantum circuits, *PRX Quantum* **2**, 010329 (2021).
- [25] S. F. E. Oliviero, L. Leone, A. Hamma, and S. Lloyd, Measuring magic on a quantum processor, *npj Quantum Information* **8**, [10.1038/s41534-022-00666-5](https://doi.org/10.1038/s41534-022-00666-5) (2022).
- [26] P. Niroula, C. D. White, Q. Wang, S. Johri, D. Zhu, C. Monroe, C. Noel, and M. J. Gullans, Phase transition in magic with random quantum circuits (2023), [arXiv:2304.10481](https://arxiv.org/abs/2304.10481) [quant-ph].
- [27] V. Veitch, S. H. Mousavian, D. Gottesman, and J. Emerson, The resource theory of stabilizer quantum computation, *New J. Phys.* **16**, 013009 (2014).
- [28] S. Bravyi and A. Kitaev, Universal quantum computation with ideal Clifford gates and noisy ancillas, *Phys. Rev. A* **71**, 022316 (2005).
- [29] L. Leone, S. F. E. Oliviero, and A. Hamma, Stabilizer Renyi Entropy, *Phys. Rev. Lett.* **128**, 050402 (2022).
- [30] Z.-W. Liu and A. Winter, Many-Body Quantum Magic, *PRX Quantum* **3**, 020333 (2022).
- [31] S. Aaronson and D. Gottesman, Improved simulation of stabilizer circuits, *Physical Review A* **70**, [10.1103/physreva.70.052328](https://doi.org/10.1103/physreva.70.052328) (2004).
- [32] M. Yoganathan, R. Jozsa, and S. Strelchuk, Quantum advantage of unitary Clifford circuits with magic state inputs, *Proceedings of the Royal Society A* **475**, 20180427 (2019).
- [33] A. Gu, S. F. E. Oliviero, and L. Leone, Doped stabilizer states in many-body physics and where to find them (2024), [arXiv:2403.14912](https://arxiv.org/abs/2403.14912) [quant-ph].
- [34] H. Pashayan, O. Reardon-Smith, K. Korzekwa, and S. D. Bartlett, Fast Estimation of Outcome Probabilities for Quantum Circuits, *PRX Quantum* **3**, 020361 (2022).
- [35] X. Turkeshi, M. Schirò, and P. Sierant, Measuring non-stabilizerness via multifractal flatness, *Phys. Rev. A* **108**, 042408 (2023).
- [36] L. Leone, S. F. E. Oliviero, Y. Zhou, and A. Hamma, Quantum Chaos is Quantum, *Quantum* **5**, 453 (2021).
- [37] T. Haug, S. Lee, and M. Kim, Efficient stabilizer entropies for quantum computers, [arXiv:2305.19152](https://arxiv.org/abs/2305.19152) (2023).
- [38] E. Tirrito, P. S. Tarabunga, G. Lami, T. Chanda, L. Leone, S. F. E. Oliviero, M. Dalmonte, M. Collura, and A. Hamma, Quantifying non-stabilizerness through entanglement spectrum flatness (2023), [arXiv:2304.01175](https://arxiv.org/abs/2304.01175) [quant-ph].
- [39] S. Garnerone, T. R. de Oliveira, and P. Zanardi, Typicality in random matrix product states, *Physical Review A* **81**, [10.1103/physreva.81.032336](https://doi.org/10.1103/physreva.81.032336) (2010).
- [40] S. Garnerone, T. R. de Oliveira, S. Haas, and P. Zanardi, Statistical properties of random matrix product states, *Physical Review A* **82**, [10.1103/physreva.82.052312](https://doi.org/10.1103/physreva.82.052312) (2010).
- [41] D. Haag, F. Baccari, and G. Styliaris, Typical Correlation Length of Sequentially Generated Tensor Network States, *PRX Quantum* **4**, [10.1103/prxquantum.4.030330](https://doi.org/10.1103/prxquantum.4.030330) (2023).
- [42] J. Haferkamp, C. Bertoni, I. Roth, and J. Eisert, Emergent Statistical Mechanics from Properties of Disordered Random Matrix Product States, *PRX Quantum* **2**, [10.1103/prxquantum.2.040308](https://doi.org/10.1103/prxquantum.2.040308) (2021).
- [43] C. Lancien and D. Pérez-García, Correlation length in random mps and peps, *Annales Henri Poincaré* **23**, 141–222 (2021).
- [44] L. Chen, R. J. Garcia, K. Bu, and A. J. Jaffe, Magic of Random Matrix Product States (2022), [arXiv:2211.10350](https://arxiv.org/abs/2211.10350).
- [45] M. P. Fisher, V. Khemani, A. Nahum, and S. Vijay, Random quantum circuits, *Annual Review of Condensed Matter Physics* **14**, 335–379 (2023).
- [46] D. Gross, S. Nezami, and M. Walter, Schur–weyl duality for the clifford group with applications: Property testing, a robust hudson theorem, and de finetti representations, *Communications in Mathematical Physics* **385**, 1325 (2021).
- [47] R. O. P. Damanik, Optimality in Stabilizer Testing, Report, August (2018).
- [48] A. A. Mele, Introduction to Haar Measure Tools in Quantum Information: A Beginner’s Tutorial (2024), [arXiv:2307.08956](https://arxiv.org/abs/2307.08956) [quant-ph].
- [49] D. Gross, K. Audenaert, and J. Eisert, Evenly distributed unitaries: On the structure of unitary designs, *Journal of Mathematical Physics* **48**, [10.1063/1.2716992](https://doi.org/10.1063/1.2716992) (2007).
- [50] M. Ippoliti and W. W. Ho, Solvable model of deep thermalization with distinct design times, *Quantum* **6**, 886 (2022).
- [51] Z. Webb, The Clifford group forms a unitary 3-design (2016), [arXiv:1510.02769](https://arxiv.org/abs/1510.02769) [quant-ph].
- [52] G. Köstenberger, Weingarten Calculus (2021), [arXiv:2101.00921](https://arxiv.org/abs/2101.00921) [math.PR].
- [53] M. Howard and E. Campbell, Application of a resource theory for magic states to fault-tolerant quantum computing, *Physical Review Letters* **118**, [10.1103/physrevlett.118.090501](https://doi.org/10.1103/physrevlett.118.090501) (2017).
- [54] T. Haug and M. Kim, Scalable Measures of Magic Resource for Quantum Computers, *PRX Quantum* **4**, 010301 (2023).

- [55] S. F. E. Oliviero, L. Leone, and A. Hamma, Magic-state resource theory for the ground state of the transverse-field Ising model, *Phys. Rev. A* **106**, 042426 (2022).
- [56] G. Passarelli, R. Fazio, and P. Lucignano, Nonstabilizerness of permutationally invariant systems (2024), [arXiv:2402.08551 \[quant-ph\]](https://arxiv.org/abs/2402.08551).
- [57] G. Lami and M. Collura, Nonstabilizerness via Perfect Pauli Sampling of Matrix Product States, *Phys. Rev. Lett.* **131**, 180401 (2023).
- [58] G. Lami and M. Collura, Learning the stabilizer group of a Matrix Product State (2024), [arXiv:2401.16481 \[quant-ph\]](https://arxiv.org/abs/2401.16481).
- [59] T. Haug and L. Piroli, Quantifying nonstabilizerness of matrix product states, *Physical Review B* **107**, 10.1103/physrevb.107.035148 (2023).
- [60] T. Haug and L. Piroli, Stabilizer entropies and nonstabilizerness monotonies, *Quantum* **7**, 1092 (2023).
- [61] P. S. Tarabunga, E. Tirrito, M. C. Bañuls, and M. Dalmonte, Nonstabilizerness via matrix product states in the Pauli basis (2024), [arXiv:2401.16498 \[quant-ph\]](https://arxiv.org/abs/2401.16498).
- [62] D. Rattacaso, L. Leone, S. F. E. Oliviero, and A. Hamma, Stabilizer entropy dynamics after a quantum quench, *Phys. Rev. A* **108**, 042407 (2023).
- [63] P. S. Tarabunga, E. Tirrito, T. Chanda, and M. Dalmonte, Many-Body Magic Via Pauli-Markov Chains—From Criticality to Gauge Theories, *PRX Quantum* **4**, 040317 (2023).
- [64] G. E. Fux, E. Tirrito, M. Dalmonte, and R. Fazio, Entanglement-magic separation in hybrid quantum circuits (2023), [arXiv:2312.02039 \[quant-ph\]](https://arxiv.org/abs/2312.02039).
- [65] X. Turkeshi, A. Dymarsky, and P. Sierant, Pauli Spectrum and Magic of Typical Quantum Many-Body States (2023), [arXiv:2312.11631 \[quant-ph\]](https://arxiv.org/abs/2312.11631).
- [66] L. Leone and L. Bittel, Stabilizer entropies are monotonies for magic-state resource theory (2024), [arXiv:2404.11652 \[quant-ph\]](https://arxiv.org/abs/2404.11652).
- [67] C. Schon, E. Solano, F. Verstraete, J. I. Cirac, and M. M. Wolf, Sequential Generation of Entangled Multiqubit States, *Phys. Rev. Lett.* **95**, 110503 (2005).
- [68] S.-H. Lin, R. Dilip, A. G. Green, A. Smith, and F. Pollmann, Real- and Imaginary-Time Evolution with Compressed Quantum Circuits, *PRX Quantum* **2**, 10.1103/prxquantum.2.010342 (2021).
- [69] M. S. Rudolph, J. Chen, J. Miller, A. Acharya, and A. Perdomo-Ortiz, Decomposition of Matrix Product States into Shallow Quantum Circuits (2022), [arXiv:2209.00595 \[quant-ph\]](https://arxiv.org/abs/2209.00595).
- [70] G. Lami, P. Torta, G. E. Santoro, and M. Collura, Quantum annealing for neural network optimization problems: A new approach via tensor network simulations, *SciPost Physics* **14**, 10.21468/scipostphys.14.5.117 (2023).
- [71] D. Malz, G. Styliaris, Z.-Y. Wei, and J. I. Cirac, Preparation of Matrix Product States with Log-Depth Quantum Circuits, *Phys. Rev. Lett.* **132**, 040404 (2024).
- [72] K. C. Smith, A. Khan, B. K. Clark, S. M. Girvin, and T.-C. Wei, Constant-depth preparation of matrix product states with adaptive quantum circuits (2024), [arXiv:2404.16083 \[quant-ph\]](https://arxiv.org/abs/2404.16083).
- [73] D. Maslov and M. Roetteler, Shorter stabilizer circuits via Bruhat decomposition and quantum circuit transformations, *IEEE Transactions on Information Theory* **64**, 4729 (2018).
- [74] R. Cleve, D. Leung, L. Liu, and C. Wang, Near-linear constructions of exact unitary 2-designs, [arXiv:1501.04592](https://arxiv.org/abs/1501.04592) (2015).
- [75] M. Ippoliti and W. W. Ho, Dynamical purification and the emergence of quantum state designs from the projected ensemble, *PRX Quantum* **4**, 030322 (2023).
- [76] A. Paviglianiti, G. Lami, M. Collura, and A. Silva, Estimating Non-Stabilizerness Dynamics Without Simulating It (2024), in preparation.
- [77] S. True and A. Hamma, Transitions in Entanglement Complexity in Random Circuits, *Quantum* **6**, 818 (2022).
- [78] Y. Cao, J. Romero, J. P. Olson, M. Degroote, P. D. Johnson, M. Kieferová, I. D. Kivlichan, T. Menke, B. Peropadre, N. P. Sawaya, *et al.*, Quantum chemistry in the age of quantum computing, *Chemical reviews* **119**, 10856 (2019).
- [79] C. W. Bauer, Z. Davoudi, A. B. Balantekin, T. Bhattacharya, M. Carena, W. A. De Jong, P. Draper, A. El-Khadra, N. Gemelke, M. Hanada, *et al.*, Quantum simulation for high-energy physics, *PRX quantum* **4**, 027001 (2023).
- [80] H.-Y. Huang, Y. Liu, M. Broughton, I. Kim, A. Anshu, Z. Landau, and J. R. McClean, Learning shallow quantum circuits, [arXiv:2401.10095](https://arxiv.org/abs/2401.10095) (2024).



## SUPPLEMENTARY MATERIALS

### Appendix A: Haar averages

In this Appendix, we present additional calculations for the Haar average of the linearized magic and for the purity fluctuations.

#### 1 Haar average of magic

Here we derive the average value of the linearized magic  $m_n(|\phi\rangle) = \|\Pi_\phi\|_n^n$  for Haar states. Using the Haar average formula  $\mathbb{E}_{\phi \sim \mu_H} [(|\phi\rangle\langle\phi|)^{\otimes k}] = P_{\text{symm}}^{(k)} / \text{Tr}[P_{\text{symm}}^{(k)}]$ , we have:

$$\mathbb{E}_{\phi \sim \mu_H} [\|\Pi_\phi\|_n^n] = d^{-n} \sum_{\sigma \in \tilde{\mathcal{P}}_N} \mathbb{E}_{\phi \sim \mu_H} [\langle \phi | \sigma | \phi \rangle^{2n}] = d^{-n} (\text{Tr}[P_{\text{symm}}^{(k)}])^{-1} \sum_{\sigma \in \tilde{\mathcal{P}}_N} \text{Tr}[\sigma P_{\text{symm}}^{(k)}], \quad (\text{A1})$$

where  $k = 2n$ . The trace of an operator times the symmetric projector  $P_{\text{symm}}^{(k)}$  can be systematically computed by counting the length of cycles associated to each permutation in  $S_k$  [52]. The result is

$$\text{Tr}[\sigma P_{\text{symm}}^{(4)}] = \frac{1}{4!} \left( \text{Tr}[\sigma]^4 + 6 \text{Tr}[\sigma]^2 \text{Tr}[\sigma^2] + 3 \text{Tr}[\sigma^2]^2 + 8 \text{Tr}[\sigma] \text{Tr}[\sigma^3] + 6 \text{Tr}[\sigma^4] \right) \quad (\text{A2})$$

for  $n = 2$ , and a similar (but longer) expression for  $n = 3$ . The summation over  $\sigma \in \tilde{\mathcal{P}}_N$  splits into the identity  $\sigma = \mathbb{1}$  plus all others  $(d^2 - 1)$  Pauli strings  $\sigma \neq \mathbb{1}$  (which give the same contribution). Finally one obtain:

$$\mathbb{E}_{\phi \sim \mu_H} [\|\Pi_\phi\|_2^2] = \frac{1}{d^2} \left( 1 + 3 \frac{d-1}{d+3} \right). \quad (\text{A3})$$

For the case  $n = 3$  instead

$$\mathbb{E}_{\phi \sim \mu_H} [\|\Pi_\phi\|_3^3] = \frac{1}{d^3} \left( 1 + \frac{15(d-1)}{(3+d)(5+d)} \right). \quad (\text{A4})$$

Notice that in the limit of large system size one finds

$$\lim_{d \rightarrow \infty} \left( d^n \mathbb{E}_{\phi \sim \mu_H} [\|\Pi_\phi\|_n^n] \right) = \begin{cases} 4, & \text{if } n = 2 \\ 1, & \text{if } n = 3 \end{cases}. \quad (\text{A5})$$

#### 2 Haar average of purity fluctuations

Here we derive the average value of purity fluctuations for Haar states, which is defined as

$$\Delta^2 P_A(|\psi\rangle) \Big|_H = \mathbb{E}_{\psi \sim \mu_H} [P_A(|\psi\rangle)^2] - \mathbb{E}_{\psi \sim \mu_H} [P_A(|\psi\rangle)]^2. \quad (\text{A6})$$

The second term is the square of the average purity, and has already been computed in the main text (Eq. 5), obtaining:

$$\mathbb{E}_{\psi \sim \mu_H} [P_A(|\psi\rangle)]^2 = \left( \frac{d_A + d_B}{d_A d_B + 1} \right)^2 = \frac{4d}{(d+1)^2}, \quad (\text{A7})$$

where we set  $d_A = d_B = d^{1/2}$ . The first term gives instead

$$\begin{aligned} \mathbb{E}_{\psi \sim \mu_H} [P_A(|\psi\rangle)^2] &= \mathbb{E}_{\psi \sim \mu_H} \left[ \text{Tr} \left[ \rho^{\otimes 4} T_{2143}^{(A)} \right] \right] = \frac{1}{\text{Tr} \left[ P_{\text{symm}}^{(4)} \right]} \text{Tr} \left[ P_{\text{symm}}^{(4)} T_{2143}^{(A)} \right] = \\ &= \frac{1}{d(d+1)(d+2)(d+3)} \sum_{\pi \in S_4} \left( \text{Tr}_A [T_\pi^{(A)} T_{2143}^{(A)}] \text{Tr}_B [T_\pi^{(B)}] \right), \end{aligned} \quad (\text{A8})$$

where  $\rho = |\psi\rangle\langle\psi|$  and we used the fact that every permutation  $T_\pi$  can be split as  $T_\pi = T_\pi^{(A)} \otimes T_\pi^{(B)}$ . The term  $\text{Tr}_A[T_\pi^{(A)}T_{2143}^{(A)}]$  can be rewritten as  $\langle\langle T_\pi^{(A)}|T_{2143}^{(A)}\rangle\rangle$ , where permutation operators reshaped into vector states. Consequently, one needs to calculate the overlaps of these permutation vectors. This calculation can be efficiently performed using permutation formalism, which involves merely counting the permutation cycles (see Ref. [41, 44, 48] for details). By explicitly evaluating all contributions in the sum, we obtain (again with  $d_A = d_B = d^{1/2}$ )

$$\mathbb{E}_{\psi \sim \mu_H} [\text{P}_A(|\psi\rangle)^2] = \frac{2 + 18d + 4d^2}{(d+1)(d+2)(d+3)}, \quad (\text{A9})$$

and finally

$$\Delta^2 \text{P}_A(|\psi\rangle)|_H = \frac{2(d-1)^2}{(d+1)^2(d+2)(d+3)}. \quad (\text{A10})$$

Notice that for large  $d$ ,  $\Delta^2 \text{P}_A(|\psi\rangle)|_H \sim \mathcal{O}(d^{-2})$ .

## Appendix B: Clifford averages

### 1 Frame potential

Here we derive the expression for the frame potential  $\mathcal{F}^{(4)}$  of any ensemble of states of the form  $\mathcal{U}_c |\phi\rangle$ . We have to evaluate

$$\mathcal{F}^{(4)} = \mathbb{E}_{\mathcal{U}_c, \mathcal{V}_c \sim \mu_C} [\text{Tr}[(\mathcal{U}_c^\dagger |\phi\rangle\langle\phi| \mathcal{U}_c)^{\otimes 4} (\mathcal{V}_c^\dagger |\varphi\rangle\langle\varphi| \mathcal{V}_c)^{\otimes 4}]], \quad (\text{B1})$$

where  $|\phi\rangle, |\varphi\rangle$  are fixed states. Now we use the expression of the 4-fold Clifford channel

$$\mathbb{E}_{\mathcal{U}_c \sim \mu_C} [(\mathcal{U}_c^\dagger |\phi\rangle\langle\phi| \mathcal{U}_c)^{\otimes 4}] = \alpha_\phi Q P_{\text{symm}}^{(4)} + \beta_\phi P_{\text{symm}}^{(4)} \quad \mathbb{E}_{\mathcal{U}_c \sim \mu_C} [(\mathcal{U}_c^\dagger |\varphi\rangle\langle\varphi| \mathcal{U}_c)^{\otimes 4}] = \alpha_\varphi Q P_{\text{symm}}^{(4)} + \beta_\varphi P_{\text{symm}}^{(4)} \quad (\text{B2})$$

with the coefficients  $\alpha_\phi, \beta_\phi, \alpha_\varphi, \beta_\varphi$  defined as in Eq. 7. We now need to compute traces of products of operators like  $\text{Tr}[P_{\text{symm}}^{(4)} P_{\text{symm}}^{(4)}]$ ,  $\text{Tr}[P_{\text{symm}}^{(4)} Q P_{\text{symm}}^{(4)}]$ , etc. The calculation simplifies greatly using the cyclicity of the trace, the fact that  $P$  and  $Q$  are projectors ( $(P_{\text{symm}}^{(4)})^2 = P_{\text{symm}}^{(4)}$ ,  $Q^2 = Q$ ), and  $[Q, T_\pi] = 0$  [36]. The remaining traces ( $\text{Tr}[P_{\text{symm}}^{(4)}]$ ,  $\text{Tr}[P_{\text{symm}}^{(4)} Q]$ ) can be evaluated explicitly using permutation formalism [36]. The final result is

$$\mathcal{F}^{(4)} = \frac{6(d^2 \|\Pi_\phi\|_2^2 \|\Pi_\varphi\|_2^2 + 3d \|\Pi_\phi\|_2^2 \|\Pi_\varphi\|_2^2 - 4 \|\Pi_\phi\|_2^2 - 4 \|\Pi_\varphi\|_2^2 + 4)}{(d-1)(d+1)(d+2)(d+4)}. \quad (\text{B3})$$

By normalizing with the fourth frame potential of Haar  $\mathcal{F}_H^{(4)}$  one gets

$$\frac{\mathcal{F}^{(4)}}{\mathcal{F}_H^{(4)}} = \frac{6d(d+3)(d^2 \|\Pi_\phi\|_2^2 \|\Pi_\varphi\|_2^2 + 3d \|\Pi_\phi\|_2^2 \|\Pi_\varphi\|_2^2 - 4 \|\Pi_\phi\|_2^2 - 4 \|\Pi_\varphi\|_2^2 + 4)}{4(d-1)(d+4)}, \quad (\text{B4})$$

and thus

$$(\Delta^{(4)})^2 = \frac{\mathcal{F}^{(4)}}{\mathcal{F}_H^{(4)}} - 1 = \frac{(d^2 \|\Pi_\phi\|_2^2 \frac{d+3}{d} - 4)(d^2 \|\Pi_\varphi\|_2^2 \frac{d+3}{d} - 4)}{4(-1+d)(4+d)}. \quad (\text{B5})$$

As a particular case (including the average over the RMPS), we obtain Eq. 28, i.e.

$$(\Delta^{(4)})^2 = \mathbb{E}_{\phi, \varphi \sim \mu_X} \left[ \frac{(d^2 \|\Pi_\phi\|_2^2 \frac{d+3}{d} - 4)(d^2 \|\Pi_\varphi\|_2^2 \frac{d+3}{d} - 4)}{4(-1+d)(4+d)} \right] = \left( \frac{d+3}{d} \right)^2 \frac{1}{4(-1+d)(4+d)} (\delta_X^{(2)})^2. \quad (\text{B6})$$

Instead if we set  $|\phi\rangle = |\varphi\rangle = |\mathbf{0}\rangle$  we obtain the frame potential of the ensemble of pure stabilizer states [19]. In this case  $\|\Pi_\phi\|_2^2 = \|\Pi_\varphi\|_2^2 = d^{-1}$ , and therefore [19]

$$\mathcal{F}_{\text{STAB}}^{(4)} = \frac{30}{d(d+1)(d+2)(d+4)}, \quad (\Delta^{(4)})^2 = \frac{4(d-1)}{(4+d)}. \quad (\text{B7})$$

Notice that  $(\Delta^{(4)})^2 > 0$  for any  $d > 1$ , meaning that stabilizer states does not constitute an exact 4-design.

## 2 Clifford average of purity fluctuations

Here we derive the average value of purity fluctuations for any ensemble of states of the form  $\mathcal{U}_c |\phi\rangle$ . We proceed in close similarity to what was done in Sec. A 2 for Haar. We have to compute  $\mathbb{E}_{\mathcal{U}_c \sim \mu_C} [\mathbb{P}_A(|\psi\rangle)^2]$ . By using Eqs.6,7 for the 4-fold Clifford channel, we get

$$\begin{aligned} \mathbb{E}_{\mathcal{U}_c \sim \mu_C} [\mathbb{P}_A(|\psi\rangle)^2] &= \mathbb{E}_{\mathcal{U}_c \sim \mu_C} \left[ \text{Tr} \left[ \rho^{\otimes 4} T_{2143}^{(A)} \right] \right] = \frac{1}{\text{Tr} \left[ P_{\text{symm}}^{(4)} \right]} \left( \alpha_\phi \text{Tr} \left[ P_{\text{symm}}^{(4)} T_{2143}^{(A)} \right] + \beta_\phi \text{Tr} \left[ Q P_{\text{symm}}^{(4)} T_{2143}^{(A)} \right] \right) = \\ &= \frac{1}{d(d+1)(d+2)(d+3)} \left[ \sum_{\pi \in S_4} \left( \text{Tr}_A \left[ T_\pi^{(A)} T_{2143}^{(A)} \right] \text{Tr}_B \left[ T_\pi^{(B)} \right] \right) + d^{-2} \sum_{\boldsymbol{\sigma}} \sum_{\pi \in S_4} \left( \text{Tr}_A \left[ \boldsymbol{\sigma}^{(A)} T_\pi^{(A)} T_{2143}^{(A)} \right] \text{Tr}_B \left[ \boldsymbol{\sigma}^{(B)} T_\pi^{(B)} \right] \right) \right], \end{aligned} \quad (\text{B8})$$

where  $\rho = |\psi\rangle \langle \psi| = \mathcal{U}_c^\dagger |\phi\rangle \langle \phi| \mathcal{U}_c$ . In the second line, we split the permutation  $T_\pi$  as  $T_\pi = T_\pi^{(A)} \otimes T_\pi^{(B)}$  and the Pauli string as  $\boldsymbol{\sigma} = \boldsymbol{\sigma}^{(A)} \otimes \boldsymbol{\sigma}^{(B)}$ . By explicitly evaluating the contributions given by all permutations in the sum, we obtain (again with  $d_A = d_B = d^{1/2}$ )

$$\Delta^2 \mathbb{P}_A(|\psi\rangle) = \frac{(d-1)(d^2 \|\Pi_\phi\|_2^2 + d \|\Pi_\phi\|_2^2 - 2)}{(d+1)^2(d+2)}. \quad (\text{B9})$$

As a particular case we obtain the average purity of CMPS. By using the definition of  $\delta_\chi^{(2)}$  (see Eq. 25) we obtain

$$\|\Pi_\phi\|_2^2 = \mathbb{E}_{\phi \sim \mu_H} [m_n(|\phi\rangle)] + d^{-2} \delta_\chi^{(2)}, \quad (\text{B10})$$

and by replacing the Haar averaged magic with its value (Eq. A3) we finally obtain

$$\Delta^2 \mathbb{P}_A(|\psi\rangle) = \Delta^2 \mathbb{P}_A(|\psi\rangle)|_H + \frac{(d-1)}{d(d+1)(d+2)} \delta_\chi^{(2)}. \quad (\text{B11})$$

Instead, if we set  $|\phi\rangle = |\mathbf{0}\rangle$ ,  $\|\Pi_\phi\|_2^2 = d^{-1}$ , we obtain the purity fluctuations of pure stabilizer states

$$\Delta^2 \mathbb{P}_A(|\psi\rangle)|_{\text{STAB}} = \frac{(d-1)^2}{(d+1)^2(d+2)}. \quad (\text{B12})$$

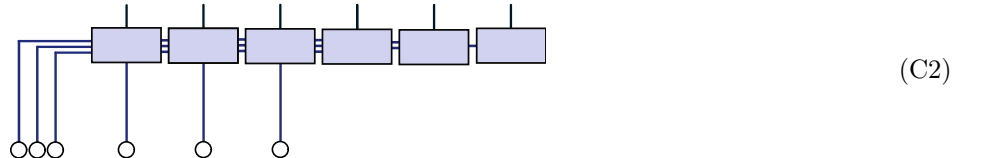
Notice that for large  $d$ ,  $\Delta^2 \mathbb{P}_A(|\psi\rangle)|_{\text{STAB}} \sim \mathcal{O}(d^{-1})$ .

### Appendix C: RMPS with open boundary conditions

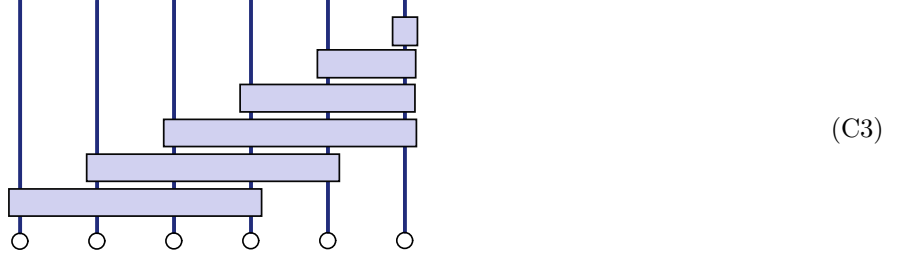
Here, we exemplify the open boundary conditions used in the quantum circuit representation of an MPS at finite system size  $N$ . In this section only, we will use the graphical convention of using single, double, triple, etc. lines to represent auxiliary bonds with dimensions 2, 4, 8,.... For illustrative purposes, we consider a particular case with  $N = 6$  qubits and maximum bond dimension  $\chi = 8$ . A right-normalized MPS is therefore



Note that it is necessary to impose a bond dimension that consecutively decreases by a factor of 2 for each of the last  $\log_2 \chi - 1$  bonds to the right. In fact, if this were not the case, the right normalization of the MPS tensors could not be fulfilled. At this point, MPS isometries  $\mathbb{A}$  can be embedded into unitary gates provided an adequate number of qubits initialized to  $|0\rangle$  are supplied. This is done as follows:



Finally, the circuit can be reshaped to obtain a staircase geometry:



RMPS at finite system size are defined by using Haar-distributed unitary gates in the circuit. Notice that this construction leads to exact  $N$ -qubits Haar distribution for the final state whenever we set  $\chi = d = 2^N$  (since the unitary gate at the first layer covers all qubits in this case).

## Appendix D: Magic of RMPS

Here, we present additional results on the average RMPS of the linearized magic.

### 1 Magic of random product states ( $\chi = 1$ )

We now derive the average value of the linearized magic  $m_n(|\phi\rangle) = \|\Pi_\phi\|_n^n$  for random product states, i.e. states  $|\phi\rangle$  drawn randomly from the ensemble of RMPS with maximum bond dimension 1. We have ( $\mu_1 = \mu_{\chi=1}$ )

$$\mathbb{E}_{\phi \sim \mu_1} [\|\Pi_\phi\|_n^n] = d^{-n} \sum_{\sigma \in \tilde{\mathcal{P}}_N} \mathbb{E}_{\phi \sim \mu_1} [\langle \phi | \sigma | \phi \rangle^{2n}] = \prod_{i=1}^N \left( 2^{-n} \sum_{\sigma_i \in \tilde{\mathcal{P}}_1} \mathbb{E}_{\phi_i \sim \mu_H} [\langle \phi_i | \sigma_i | \phi_i \rangle^{2n}] \right). \quad (\text{D1})$$

For the last equality, we utilized the factorization over qubits  $i = 1 \dots N$  of both the product state  $|\phi\rangle$  and the Pauli sum, explicitly leveraging the assumption of local dimension 2. Thus, we find

$$\mathbb{E}_{\phi \sim \mu_1} [\|\Pi_\phi\|_n^n] = \left( \mathbb{E}_{\phi_i \sim \mu_1} [\|\Pi_{\phi_i}\|_n^n] \right)^N \quad (\text{D2})$$

Using Eqs. A3, A4 with  $d = 2$  to find single qubit Haar averages, one obtain (for  $n = 2, 3$ ):

$$\mathbb{E}_{\phi \sim \mu_1} [\|\Pi_\phi\|_2^2] = \frac{1}{d^2} \left( \frac{8}{5} \right)^N \quad \mathbb{E}_{\phi \sim \mu_1} [\|\Pi_\phi\|_3^3] = \frac{1}{d^3} \left( \frac{10}{7} \right)^N. \quad (\text{D3})$$

Notice that these values deviate exponentially in  $N$  from full system Haar values reported in Eqs. A3, A4. Consequently (in the limit of large  $d$ )

$$\delta_{\chi=1}^{(2)} \simeq \left( \frac{8}{5} \right)^N \quad \delta_{\chi=1}^{(3)} \simeq \left( \frac{10}{7} \right)^N. \quad (\text{D4})$$

By substituting this result into Eq. 29, one can derive the purity fluctuations for the ensemble of CMPS in the simple case  $\chi = 1$ . One obtains [36]:

$$\Delta^2 \text{P}_A(|\psi\rangle) \sim \mathcal{O}(d^{1 - \log_2 5}). \quad (\text{D5})$$

Since  $1 - \log_2 5 \simeq -1.322$ , this scaling interpolates between the result for Clifford (stabilizer) states, for which  $\Delta^2 \text{P}_A(|\psi\rangle) \sim \mathcal{O}(d^{-1})$ , and that for Haar-random states, namely  $\Delta^2 \text{P}_A(|\psi\rangle)|_{\text{H}} \sim \mathcal{O}(d^{-2})$ .

### 2 Magic of RMPS

Here we provide additional details on the evaluation of the average linearized magic  $d^n m_n(|\phi\rangle)$  for random MPS with arbitrary  $\chi$ . The calculation can be performed in two ways, corresponding to the following two ways of contracting the transfer matrices represented in Eq. 23. Method *a*) corresponds to periodic boundary conditions. Method *b*) corresponds to open boundary conditions as described in Appendix C. The latter is more accurate as it accounts for RMPS normalization.

*a Periodic boundary conditions*

We consider the transfer matrix  $\mathcal{T}$  as defined in Eq. 21 and within the bulk, specifically when the bond dimension is locally  $\chi$ , and there are no boundary effects. We define  $\lambda_\sigma$  ( $\sigma \in \{1, 2, \dots, k!\}$ ) as the eigenvalues of  $\mathcal{T}_{\sigma\pi}$ , arranged in descending order.

For  $n = 2$  ( $k = 4$  replicas), the eigenvalues  $\lambda_\sigma$  can be obtained using the symbolic computation routines of Wolfram Mathematica, and they turn out to be expressed as rational functions of  $\chi$  or roots of polynomials in  $\chi$ . It is possible to perform an expansion for large  $\chi$  and identify the leading eigenvalues. We find four leading eigenvalues converging to 1 in the large  $\chi$  limit. These are:

$$\begin{aligned}\lambda_1 &= 1 + \frac{9}{4\chi^2} - \frac{171}{16\chi^4} + \frac{5265}{64\chi^6} + \mathcal{O}\left(\frac{1}{\chi^8}\right) \\ \lambda_{2,3,4} &= 1 - \frac{3}{4\chi^2} - \frac{3}{16\chi^4} - \frac{3}{64\chi^6} + \mathcal{O}\left(\frac{1}{\chi^8}\right)\end{aligned}\tag{D6}$$

All the other eigenvalues  $\lambda_\sigma$  ( $\sigma > 4$ ) converge either to  $1/2$  or to  $1/4$ . In Fig. 2, we show the deviation of  $\lambda_1$  and  $\lambda_2 = \lambda_3 = \lambda_4$  from 1 as a function of  $\chi$  for various values of  $\chi$ . Additionally, we depict the leading term for large  $\chi$ , which in both cases scales as  $\mathcal{O}(\chi^{-2})$ . For  $n = 3$  ( $k = 6$  replicas), an exact symbolic computation of the eigenvalues is not feasible, as  $\mathcal{T}$  has a dimension of  $720 \times 720$ . However, by evaluating numerically the eigenvalues of  $\mathcal{T}$  for certain fixed values of  $\chi$ , we observe a single leading eigenvalue  $\lambda_1$  converging to 1 from above in the large  $\chi$  limit. In this case, we use a linear fit to obtain the scaling, finding

$$\lambda_1 \simeq 1 + a\chi^{-6},\tag{D7}$$

with  $a \simeq 9.70$  (see Fig. 2). All the other eigenvalues  $\lambda_\sigma$  ( $\sigma > 1$ ) converge either to  $1/2$ ,  $1/4$ ,  $1/8$  or  $1/16$ .

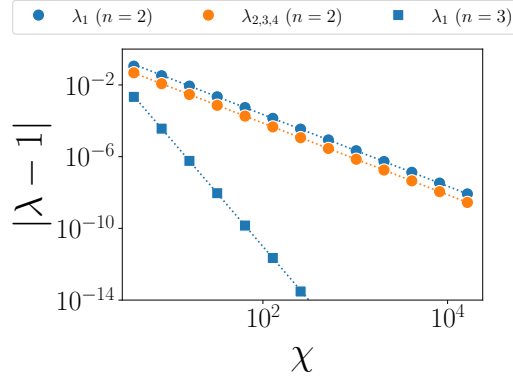


Figure 2. Leading eigenvalues of the transfer matrix  $\mathcal{T}$  in the bulk for  $n = 2$  (circles) and  $n = 3$  (squares). Straight lines represent leading term for large  $\chi$  extracted from analytical expansion ( $n = 2$ ) or from a linear fit ( $n = 3$ ).

Using these results, we find (for  $n = 2$ ):

$$\text{Tr}[\mathcal{T}^N] = \sum_{\sigma=1}^{k!} \lambda_\sigma^N \simeq \lambda_1^N + 3\lambda_2^N,\tag{D8}$$

a part for exponentially small corrections due to the others eigenvalues. By inserting Eq. D6 and taking only the leading terms for large  $N, \chi$  and small  $N/\chi^2$ , we finally get

$$\text{Tr}[\mathcal{T}^N] \simeq 4 + \frac{27}{8} \frac{N^2}{\chi^4}.\tag{D9}$$

If we define  $\delta_\chi^{(n)}$  as in Eq. 25, we assume  $d^2\mathbb{E}_{\phi \sim \mu_\chi}[m_2(|\phi\rangle)] \simeq \text{Tr}[\mathcal{T}^N]$  and we use Eq. A5 for the Haar value, we obtain

$$\delta_\chi^{(2)} \sim \mathcal{O}\left(\frac{N^2}{\chi^4}\right).\tag{D10}$$

Similarly, one finds

$$\delta_\chi^{(3)} \sim \mathcal{O}\left(\frac{N}{\chi^6}\right). \quad (\text{D11})$$

In Fig. 3, panels *a*) and *b*), display the computed values of  $\delta_\chi^{(n)}$  using the expression  $\text{Tr}[\mathcal{T}^N] = \sum_{\sigma=1}^{k!} \lambda_\sigma^N$ , where the eigenvalues  $\lambda_\sigma$  have been numerically determined for increasing values of  $\chi$  and  $n = 2, 3$ . Through a linear fit (dotted lines), we find

$$\delta_\chi^{(2)} \simeq a\chi^{-2} \quad \delta_\chi^{(3)} \simeq a\chi^{-6}. \quad (\text{D12})$$

Subsequent fitting (see panels *c*) and *d*)) reveals that the coefficient  $a$  exhibits quadratic dependence on  $N$  for  $n = 2$  and linear dependence for  $n = 3$ . Collectively, these results corroborate the analytical predictions specified in Eqs. D10 and D11.

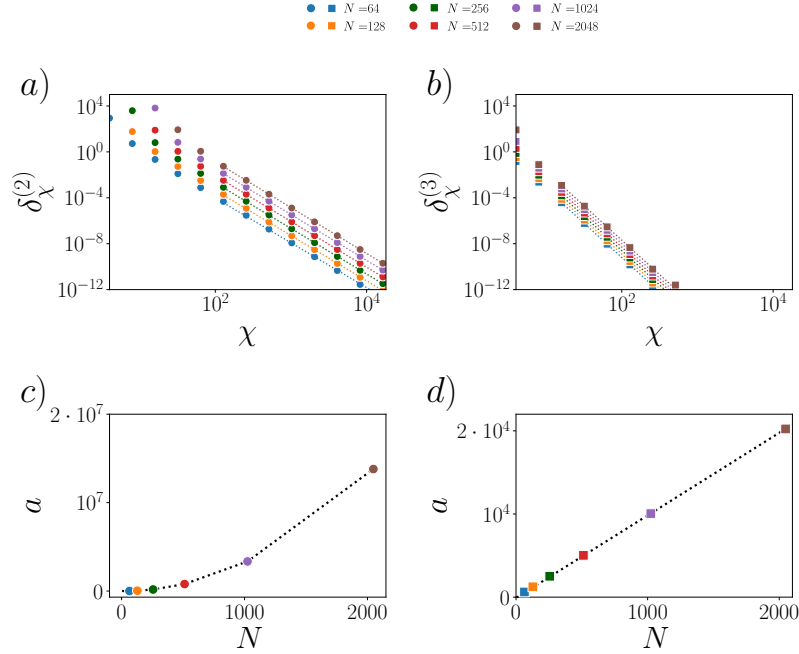


Figure 3. Upper panels: magic deviation from Haar  $\delta_\chi^{(n)}$  for RMPS at finite size  $N$  and  $n = 2$  (*a*),  $n = 3$  (*b*). Here, we employ periodic boundary conditions, see Eq. 23 *a*). Dotted lines represent the linear fit in log log scale (Eq.D12). Lower panels: coefficients  $a$  as a function of  $N$  for  $n = 2$  (*c*),  $n = 3$  (*d*).

### *b* Open boundary conditions

In Fig. 4, panels *a*) and *b*), we plot the magic deviation from Haar  $\delta_\chi^n$  ( $n = 2, 3$ ) for RMPS at finite system size and open boundary conditions. Transfer matrices  $\mathcal{T}$  are site dependent and contracted as in Eq.23. Boundary conditions are implemented as discussed in Section C.

Through a linear fit (dotted lines), we find

$$\delta_\chi^{(2)} \simeq a\chi^{-2} \quad \delta_\chi^{(3)} \simeq a\chi^{-3}. \quad (\text{D13})$$

Subsequent fitting (see panels *c*) and *d*)) reveals that the coefficient  $a$  exhibits linear dependence for both  $n = 2$  and  $n = 3$ . This reveals that the correct scaling of the magic deviation from Haar is

$$\delta_\chi^{(2)} \sim \mathcal{O}\left(\frac{N}{\chi^2}\right) \quad \delta_\chi^{(3)} \sim \mathcal{O}\left(\frac{N}{\chi^3}\right). \quad (\text{D14})$$

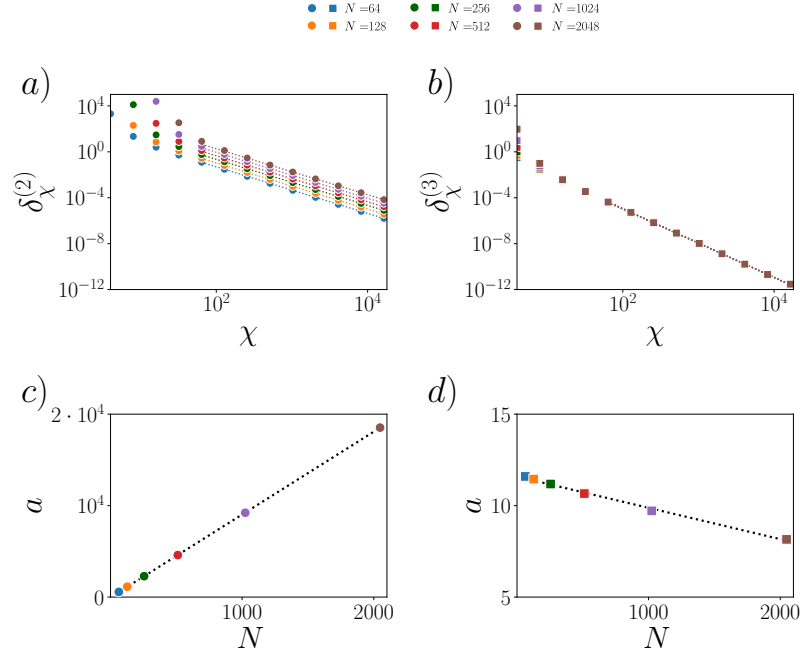


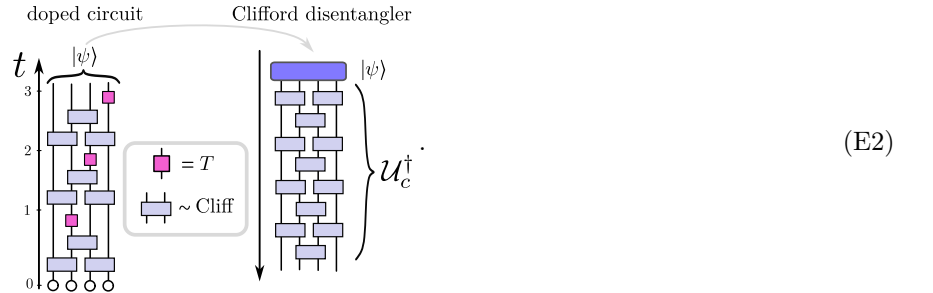
Figure 4. Upper panels: magic deviation from Haar  $\delta_\chi^{(n)}$  for RMPS at finite size  $N$  and  $n = 2$  (a),  $n = 3$  (b). Here, we employ open boundary conditions, see Eq. 23 b). Dotted lines represent the linear fit in log log scale (Eq.D13). Lower panels: coefficients  $a$  as a function of  $N$  for  $n = 2$  (c),  $n = 3$  (d).

### Appendix E: CMPS and entanglement cooling

We now describe and test an algorithm aimed at finding the optimal Clifford unitary  $\mathcal{U}_c^\dagger$  to disentangle a given state  $|\psi\rangle$ . The goal is to find an approximate CMPS decomposition, i.e.

$$|\psi\rangle \simeq \mathcal{U}_c |\phi\rangle_\chi \quad (\text{E1})$$

where  $|\phi\rangle_\chi$  is a suitable MPS, with (small) bond dimension  $\chi$ . The approach is known as entanglement cooling [77]. Essentially, one applies two-local Clifford gates to  $|\psi\rangle$ , optimizing each gate to minimize the entanglement entropy between qubits  $[1, i]$  and  $[i + 1, N]$ . Given that the size of the two-qubit Clifford group is  $|\mathcal{C}(4)| = 11520$ , the optimal Clifford gate can be determined numerically through a brute-force search. After identifying the optimal gate, the process is repeated sequentially for the next bonds, and additional layers of Clifford gates are optimized in a similar manner. The algorithm ultimately outputs an optimized disentangling Clifford circuit of a specific depth. Extensions of the algorithm with finite-temperature stochastic optimization of local Clifford gates can be also considered [77]. Here, we bench-mark the algorithm on states  $|\psi\rangle$  resulting from random Clifford circuits doped with  $T$  gates. Specifically, we construct  $|\psi\rangle$  by alternating brick wall layers of random two-qubit Clifford gates with a single  $T$  gate placed at a random position. Afterwards we apply entanglement cooling on  $|\psi\rangle$ , as illustrated here:



Note that the discrete time of the circuit is conventionally taken to be 1 when  $v$  brick wall layers of local Clifford gates have been applied, followed by one  $T$  gate. Physically,  $v$  represents the circuit's light velocity ( $v = 1$  in the picture).

In Fig. 5, we show results for system of size  $N = 6, 8, 10, 12$  and  $10^2$  random realizations of the doped circuit. The depth of the Clifford disentangling circuit is set to  $N$ . We plot the entanglement entropy of the state  $|\psi\rangle$  resulting from the doped circuit (solid lines), and entanglement entropy of the disentangled state  $\mathcal{U}_c^\dagger |\psi\rangle$  (dotted lines). The entanglement entropy  $S$  is maximized across system bipartitions and averaged over circuit realizations. In the plot, we scale  $S$  as  $S/N$ , and the circuit time  $t$  as  $vt/N$ . Our results suggest that doped circuits with  $vt/N \lesssim 1$  can be effectively disentangled using Clifford operations. However, for  $vt/N \gtrsim 1$ , this method becomes progressively less effective. The entanglement entropy of the disentangled state  $\mathcal{U}_c^\dagger |\psi\rangle$  appears to follow a volume law, as evidenced by the converging curves of  $S/N$ . This suggests that entanglement cooling may not be suitable for finding an optimal CMPS representation. Indeed, the findings of this paper indicate that a CMPS representation for generic states  $|\psi\rangle$  can potentially be achieved with an MPS of bond dimension  $\mathcal{O}(N^{1/2})$ , corresponding to an entanglement  $S \sim \mathcal{O}(\log N)$ .

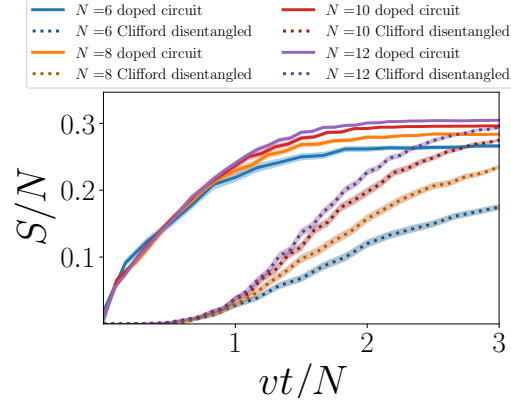


Figure 5. Entanglement cooling is applied to doped circuit (see Eq. E2). Continuous lines represent entanglement of the final state  $|\psi\rangle$ , dotted lines the entanglement of the Clifford disentangled state  $\mathcal{U}_c^\dagger |\psi\rangle$ .